

# Parisite-(La), ideally $\text{CaLa}_2(\text{CO}_3)_3\text{F}_2$ , a new mineral from Novo Horizonte, Bahia, Brazil

LUIZ A. D. MENEZES FILHO<sup>1,†</sup>, MARIO L. S. C. CHAVES<sup>1</sup>, NIKITA V. CHUKANOV<sup>2</sup>, DANIEL ATENCIO<sup>3,\*</sup>, RICARDO SCHOLZ<sup>4</sup>, IGOR PEKOV<sup>5</sup>, GERALDO MAGELA DA COSTA<sup>6</sup>, SHAUNNA M. MORRISON<sup>7</sup>, MARCELO B. ANDRADE<sup>8</sup>, ERICO T. F. FREITAS<sup>9</sup>, ROBERT T. DOWNS<sup>7</sup> AND DMITRIY I. BELAKOVSKIY<sup>10</sup>

<sup>1</sup> Universidade Federal de Minas Gerais (UFMG), Instituto de Geociências, Departamento de Geologia, Avenida Antônio Carlos, 6627, 31270-901, Belo Horizonte, MG, Brazil

<sup>2</sup> Institute of Problems of Chemical Physics, Russian Academy of Sciences, Chernogolovka, Moscow region, 142432 Russia

<sup>3</sup> Universidade de São Paulo, Instituto de Geociências, Rua do Lago 562, 05508-080, São Paulo, Brazil

<sup>4</sup> Universidade Federal de Ouro Preto (UFOP), Escola de Minas, Departamento de Geologia, Campus Morro do Cruzeiro, 35400-000, Ouro Preto, MG, Brazil

<sup>5</sup> Faculty of Geology, Moscow State University, Vorobievsky Gory, Moscow, 119991 Russia

<sup>6</sup> Universidade Federal de Ouro Preto (UFOP), Instituto de Ciências Exatas e Biológicas, Departamento de Química, Campus Morro do Cruzeiro, 35400-000, Ouro Preto, MG, Brazil

<sup>7</sup> Department of Geosciences, University of Arizona, 1040 E. 4th Street, Tucson, Arizona 85721, USA.

<sup>8</sup> University of São Paulo, São Carlos Institute of Physics, PO Box 369, 13560-970, São Carlos, SP, Brazil

<sup>9</sup> Universidade Federal de Minas Gerais (UFMG), Centro de Microscopia, Avenida Antônio Carlos, 6627, 31270-901, Belo Horizonte, MG, Brazil

<sup>10</sup> Fersman Mineralogical Museum of Russian Academy of Sciences, Leninskiy Prospekt 18-2, Moscow, 119071 Russia

[Received 29 November 2016; Accepted 18 April 2017; Associate Editor: Stuart Mills]

## ABSTRACT

Parisite-(La) (IMA2016-031), ideally  $\text{CaLa}_2(\text{CO}_3)_3\text{F}_2$ , occurs in a hydrothermal vein crosscutting a metarhyolite of the Rio dos Remédios Group, at the Mula mine, Tapera village, Novo Horizonte county, Bahia, Brazil, associated with hematite, rutile, almeidaite, fluocerite-(Ce), brockite, monazite-(La), rhabdophane-(La) and bastnäsite-(La). Parisite-(La) occurs as residual nuclei (up to 5 mm) in steep doubly-terminated pseudo-hexagonal pyramidal crystals (up to 8.2 cm). Parisite-(La) is transparent, yellow-green to white, with a white streak and displays a vitreous (when yellow-green) to dull (when white) lustre. Cleavage is distinct on pseudo- $\{001\}$ ; fracture is laminated, conchoidal, or uneven. The Mohs hardness is 4 to 5, and it is brittle. Calculated density is  $4.273 \text{ g cm}^{-3}$ . Parisite-(La) is pseudo-uniaxial (+),  $\omega = 1.670(2)$  and  $\epsilon = 1.782(5)$  (589 nm). The empirical formula normalized on the basis of 11 (O + F) atoms per formula unit (apfu) is  $\text{Ca}_{0.98}(\text{La}_{0.83}\text{Nd}_{0.51}\text{Ce}_{0.37}\text{Pr}_{0.16}\text{Sm}_{0.04}\text{Y}_{0.03})_{\Sigma 1.94}\text{C}_{3.03}\text{O}_{8.91}\text{F}_{2.09}$ . The IR spectrum confirms the absence of OH groups. Single-crystal X-ray studies gave the following results: monoclinic (pseudo-trigonal), space group:  $C2$ ,  $Cm$ , or  $C2/m$ ,  $a = 12.356(1) \text{ \AA}$ ,  $b = 7.1368(7) \text{ \AA}$ ,  $c = 28.299(3) \text{ \AA}$ ,  $\beta = 98.342(4)^\circ$ ,  $V = 2469.1(4) \text{ \AA}^3$  and  $Z = 12$ . Parisite-(La) is the La-dominant analogue of parisite-(Ce).

**KEYWORDS:** parisite-(La), new mineral, rare-earth fluorocarbonate, Mula mine, Novo Horizonte, Bahia, Brazil.

## Introduction

\*E-mail: [datencio@usp.br](mailto:datencio@usp.br)

†Deceased July 2014

<https://doi.org/10.1180/minmag.2017.081.028>

PARISITE-(La) is the La-dominant analogue of parisite-(Ce). Minerals with a chemical composition consistent with that of parisite-(La) were

reported in several studies from different localities: Třebíč durbachite massif, SW Moravia, Czech Republic (Sulovský, 2001); at a metabauxite/marble interface in the eastern part of Samos island, Greece (Theye *et al.*, 2003); alkaline rocks in Romania (Hirtopanu, 2006, Hirtopanu *et al.*, 2015); Cerro Boggiani massif, Alto Paraguay Province, Paraguay (Enrich *et al.*, 2010); and Bear Lodge carbonatite, Wyoming, USA (Moore *et al.*, 2015). Parisite-(Nd) is also reported in literature as a mineral without IMA approval (Jambor *et al.*, 1988).

Parisite-(La) has been approved as a new mineral species by the Commission of New Minerals, Nomenclature and Classification (CNMNC) of the International Mineralogical Association (IMA 2016-031). The type specimen of parisite-(La) is deposited in the mineralogical collection of the

Museu de Geociências, Instituto de Geociências, Universidade de São Paulo, Rua do Lago, 562, 05508-080 – São Paulo, SP, Brazil, with the registration number DR1032 (a part of the holotype), and at the University of Arizona Mineral Museum (RRUFF Project deposition # R130687).

## Occurrence

Parisite-(La) occurs in a late-stage hydrothermal vein crosscutting metarhyolites, at the Mula mine, Tapera village, Novo Horizonte, State of Bahia, Brazil (12°48'28"S, 42°10'04"W). The metarhyolites, together with metadacites and meta-andesites, constitute the Rio dos Remédios Group, a package of metavolcanic acid rocks formed as a result of peraluminous and alkaline magmatism

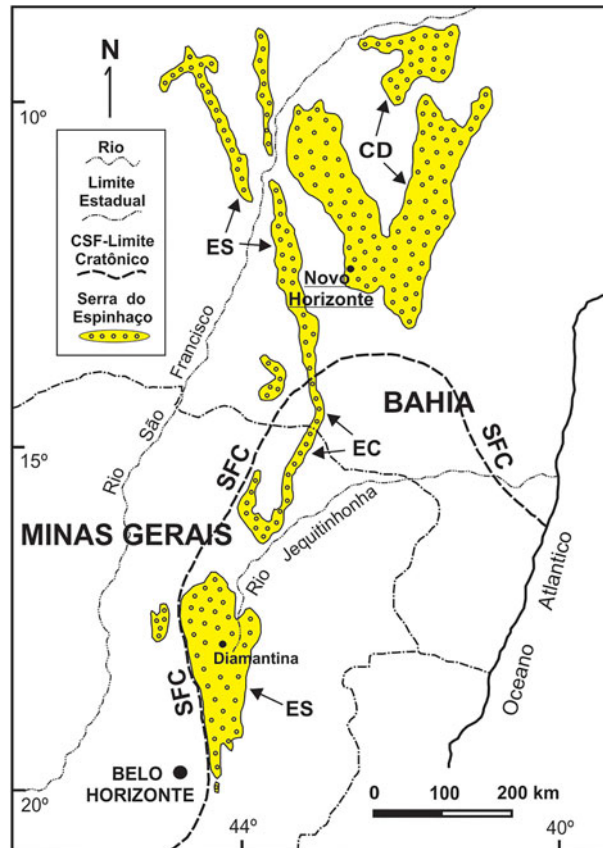


FIG. 1. The Espinhaço Range in Eastern Brazil (states of Bahia and Minas Gerais), showing its geographic/geotectonic domains Southern Espinhaço (SE), Central Espinhaço (CE), Northern Espinhaço (NE) and Chapada Diamantina (CD) in relation to the São Francisco Craton (SFC). The study area near Novo Horizonte (Bahia) is underlined.

during a continental rift which opened  $\sim 1.75$  Ga (Teixeira, 2005, Martins *et al.*, 2008). This group crops out in an area of  $\sim 35$  km  $\times$  10 km and is one of the lithologic members of a larger package of metasedimentary and locally metavolcanic rocks called Serra do Espinhaço that extends N–S for  $\sim 1200$  km from the centre of Minas Gerais to the northern reaches of Bahia state (Fig. 1). The evolution of the sedimentary basin in this region occurred in several stages during the Mesoproterozoic ( $\sim 1.7$ – $1.2$  Ga) and during subsequent metamorphism, folding and fracturing, during the Brasiliano Cycle of the Neoproterozoic (630–490 Ma, according to Pedrosa-Soares *et al.*, 2011). During the Brasiliano event, swarms of hydrothermal quartz veins were generated. These have been exploited at Novo Horizonte for the production of rutiled quartz, barite and gold. Martins *et al.* (2008) reported muscovite ages of 404 and 490 Ma in altered metarhyolites close to these veins, confirming their formation during the Brasiliano event. Parisite-(La) is associated with almeidaite (its type locality is also the Mula mine: Menezes Filho *et al.*, 2015), hematite, rutile, fluocerite-(Ce), brockite, monazite-(La), rhabdophane-(La) and bastnäsite-(La). The pit of the Mula mine is composed of brecciated quartz veins cemented by chalcedony. The veins show a stockwork pattern, which is typical of hydraulic fracturing processes, and are partially kaolinized; their orientation is NNW–SE, with a thickness of up to 2 m.

### Appearance and physical properties

Parisite-(La) occurs as residual nuclei (up to 5 mm) in doubly-terminated pseudo-hexagonal pyramidal crystals (up to 8.2 cm) with corrugated faces (Fig. 2a,b). The crystals apparently do not differ from what is usually described for parisite-(Ce): acute dipyrramids with horizontally striated faces, terminated by a pinacoid. The pinacoid faces are cleavage planes. The crystals are prismatic in appearance due to the oscillatory combination of steep pyramids, but true prism faces are lacking or very small. However, the real forms of parisite-(La) can be pedion, pinacoid and sphenoid if the space group is  $C2$ , pedion, pinacoid and dome if  $Cm$ , or pinacoid and prism if  $C2/m$ . These crystals were partially replaced by bastnäsite-(La), monazite-(La) and rhabdophane-(La). Crusts consisting of microcrystals of parisite-(La) also occur (Fig. 2c).

Parisite-(La) is transparent, yellow–green to white, with white streak, and displays a vitreous

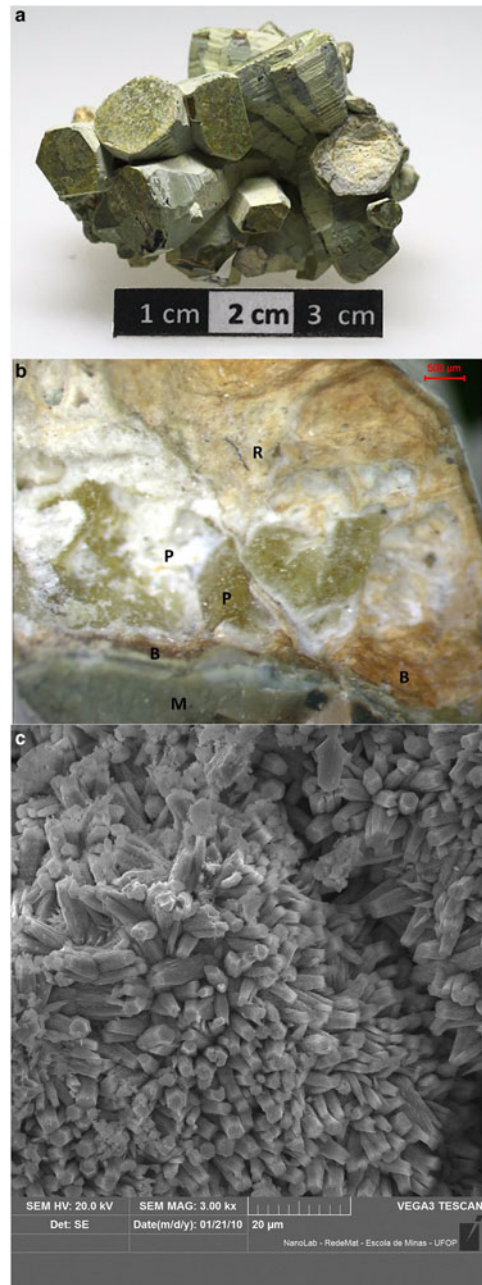


Fig. 2 (a,b) Partial pseudomorphs of monazite-(La) [M], bastnäsite-(La) [B] and rhabdophane-(La) [R] after parisite-(La) [P]. (c) Crust consisting of microcrystals of parisite-(La).

(when yellow–green) to dull (when white) lustre. It is non-fluorescent under both shortwave (254 nm) and longwave (366 nm) ultraviolet radiation.

Cleavage is distinct on pseudo- $\{001\}$  and parting was not observed; and the fracture is laminated, conchoidal, or uneven. The Mohs hardness is between 4 and 5, and the mineral is brittle. Density was not measured; the calculated density is  $4.273 \text{ g cm}^{-3}$  using the empirical formula. In transmitted light parisite-(La) is colourless, pseudo-uniaxial (+),  $\omega = 1.670(2)$  and  $\varepsilon = 1.782(5)$  (589 nm). Pleochroism was not observed.

### Infrared and Raman spectroscopy

In order to obtain infrared (IR) absorption spectra, powdered samples were mixed with anhydrous KBr, pelletized, and analysed using an ALPHA FTIR spectrometer (Bruker Optics) with the resolution of  $4 \text{ cm}^{-1}$  in the wavenumber range from  $360$  to  $3800 \text{ cm}^{-1}$ ; 16 scans were obtained. The IR spectrum of an analogous pellet of pure KBr was used as a reference. The assignments of IR

bands have been made in accordance with Adler and Kerr (1963), White (1974) and Nakamoto (1997, 2009).

The IR spectrum of parisite-(La) is close to that of parisite-(Ce) (Fig. 3). Weak IR bands in the range  $1700$ – $3000 \text{ cm}^{-1}$  correspond to overtones and combination modes. The other bands are assigned as follows ( $\text{cm}^{-1}$ ; w – weak band, s – strong band, sh – shoulder):  $1454\text{s}$ ,  $1430\text{sh}$  (degenerate asymmetric C–O-stretching vibrations),  $1089\text{w}$ ,  $1081\text{w}$  (non-degenerate symmetric C–O-stretching vibrations),  $871\text{s}$ ,  $850\text{sh}$  (out-of-plane bending vibrations of the carbonate ion triangles),  $746\text{w}$ ,  $734\text{w}$  (in-plane bending vibrations of the carbonate ion triangles),  $679\text{w}$ ,  $602\text{w}$  (presumably, overtones and/or combination modes) and  $368$  (lattice mode involving Ca–O- or REE–O-stretching vibrations where REE = rare-earth elements). Bands in the range  $3000$ – $3800 \text{ cm}^{-1}$  are not observed, which indicates the absence of OH groups.

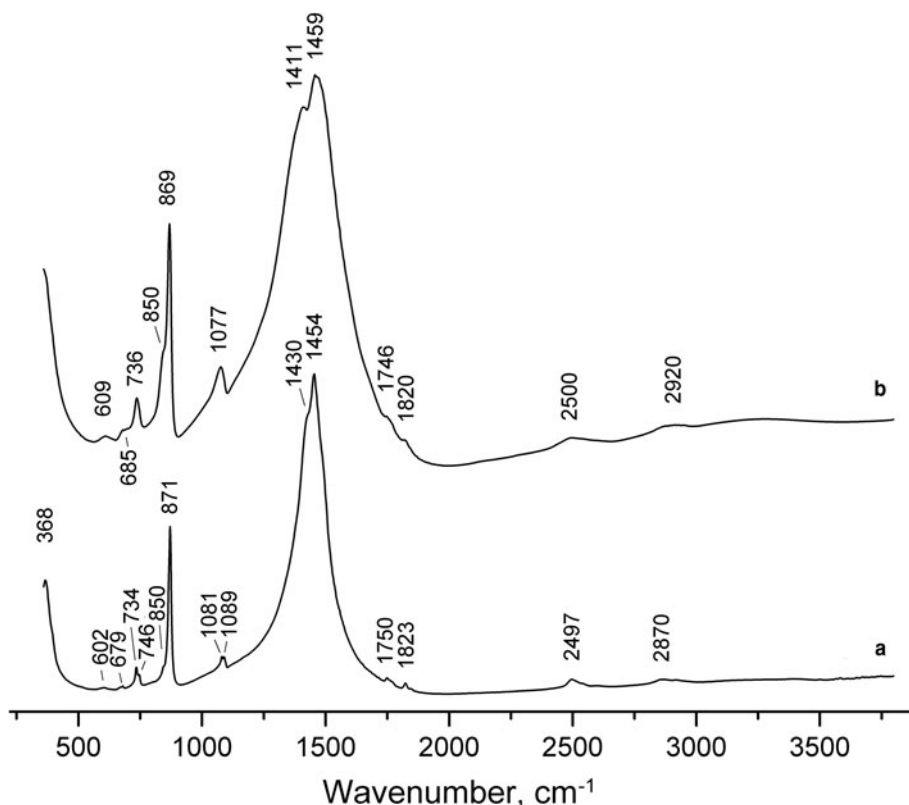


FIG. 3. Powder infrared spectra of (a) parisite-(La) and (b) parisite-(Ce) with the empirical formula  $\text{Ca}_{1.08}(\text{Ce}_{0.93}\text{La}_{0.47}\text{Nd}_{0.32}\text{Pr}_{0.06}\text{Y}_{0.08}\text{Th}_{0.06})_{\Sigma 1.92}(\text{CO}_3)_{3.00}\text{F}_{1.88}$  from White Cloud Mine, Pyrites, Ravalli Co., Montana, USA.

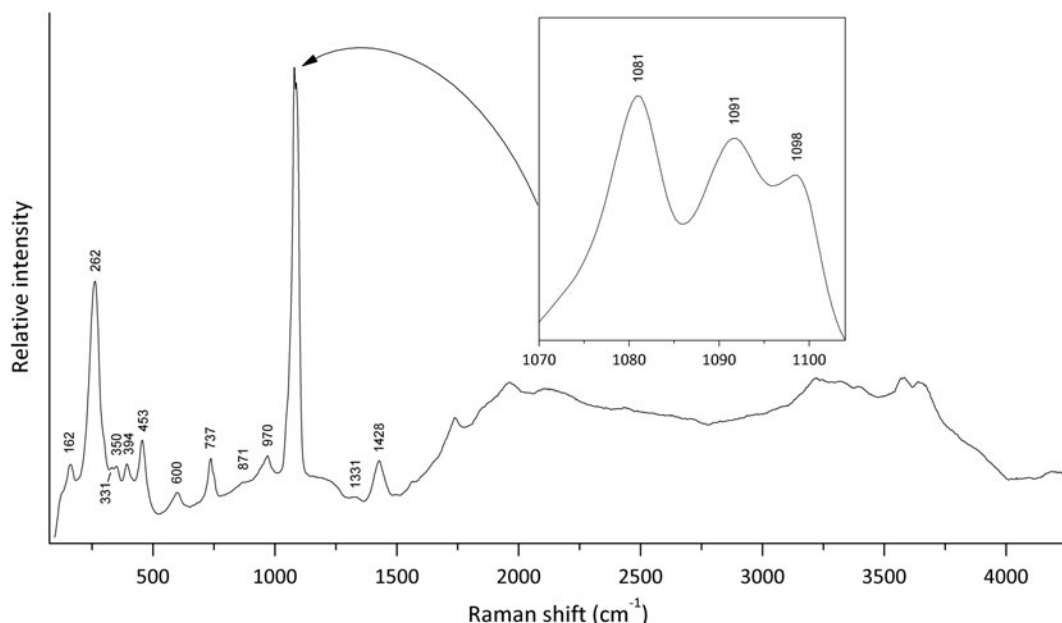


FIG. 4. Raman spectrum of parisite-(La).

The Raman spectrum of parisite-(La) (Fig. 4) was collected on a randomly oriented crystal at 100% of 150 mW on a Thermo Almega microRaman system, using a 532 nm solid-state laser, confocal Olympus optics with a 10x objective, and a thermoelectrically cooled CCD detector. The laser was partially polarized with  $4\text{ cm}^{-1}$  resolution and a spot size of  $1\ \mu\text{m}$ . The peak at  $1428\text{ cm}^{-1}$  corresponds to the  $\nu_3$  asymmetric stretching mode of  $\text{CO}_3^{2-}$  anions. Symmetric C–O stretching modes are represented by the bands at  $1081$ ,  $1091$  and  $1098\text{ cm}^{-1}$ . The bands at  $737$  and  $871\text{ cm}^{-1}$  correspond to in-plane and out-of-plane vibrations of  $\text{CO}_3^{2-}$ , respectively. The bands at  $600$  and  $970\text{ cm}^{-1}$  may be due to any vibrations involving  $\text{F}^-$  anions. Bands with wavenumbers below  $500\text{ cm}^{-1}$  are attributed to lattice modes. The tentative assignment of Raman bands is based on previous studies (Frost and Dickfos, 2007, Guastoni *et al.*, 2010, Frost *et al.*, 2013). All peaks above  $1500\text{ cm}^{-1}$  are due to fluorescence. This effect is typical for REE compounds (see e.g. Betancourt, 2003)

### Chemical data

Chemical analyses (25) were carried out using a Cameca SX100 microprobe (WDS mode, 25 kV,

40 nA and beam diameter  $5\ \mu\text{m}$ ) at the Department of Geosciences, University of Arizona, Tucson, Arizona, USA.  $\text{H}_2\text{O}$  was not analysed because of the absence of bands corresponding to O–H vibrations in the IR spectrum. The thermogravimetric (TG) curve of parisite-(La) in nitrogen atmosphere is given in Fig. 5. The second step in the TG curve may be due to the decomposition of an intermediate carbonate. Fluorine is not lost during the heating because  $\text{CaF}_2$  melts above  $1400^\circ\text{C}$  without decomposition and  $\text{REEF}_3$  do not

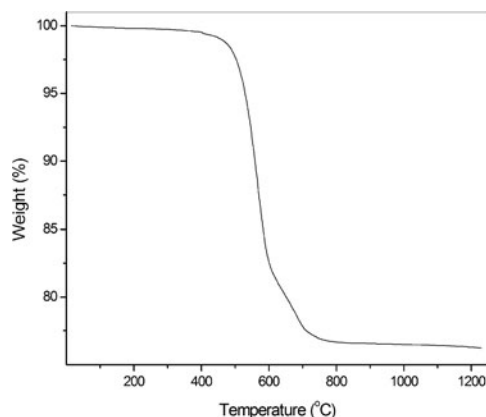


FIG. 5. Thermogravimetric curve of parisite-(La).

decompose into elements below 1200°C (Ranieri *et al.*, 2008). The formula corresponding to a CO<sub>2</sub> content of 23.68 wt.% obtained experimentally from TG data is not charge balanced. This weight loss is slightly less than 24.50 wt.% CO<sub>2</sub> calculated for formula neutrality. Mean analytical results are given in Table 1. The empirical formula normalized on the basis of 11 (O + F) apfu is Ca<sub>0.98</sub>(La<sub>0.83</sub>Nd<sub>0.51</sub>Ce<sub>0.37</sub>Pr<sub>0.16</sub>Sm<sub>0.04</sub>Y<sub>0.03</sub>)<sub>Σ1.94</sub>C<sub>3.03</sub>O<sub>8.91</sub>F<sub>2.09</sub>, where CO<sub>2</sub> was constrained to 24.50% for charge neutrality. The idealized formula is CaLa<sub>2</sub>(CO<sub>3</sub>)<sub>3</sub>F<sub>2</sub>, which requires: La<sub>2</sub>O<sub>3</sub> 60.80, CaO 10.46, CO<sub>2</sub> 24.63, F 7.09, O = F -2.98, total 100.00 wt.%.

An additional sample was measured at the Instituto de Geociências, Universidade Federal de

Minas Gerais, Belo Horizonte, Minas Gerais, Brazil. Chemical analyses (7) were carried out using a Jeol JXA8900R electron microprobe (WDS mode, 15 kV, 20 and beam diameter 5 μm). Mean analytical results are given in Table 1. The empirical formula normalized on the basis of 11 (O + F) apfu is Ca<sub>0.91</sub>(La<sub>0.82</sub>Nd<sub>0.47</sub>Ce<sub>0.43</sub>Pr<sub>0.26</sub>Sm<sub>0.04</sub>Y<sub>0.02</sub>)<sub>Σ2.04</sub>(CO<sub>3</sub>)<sub>3.03</sub>F<sub>1.91</sub>, where CO<sub>2</sub> was constrained to 24.70 wt.% for charge neutrality.

### Crystallography

Single-crystal X-ray diffraction studies and Convergent-Beam Electron Diffraction (CBED) analysis performed under transmission electron microscopy (TEM) indicated monoclinic symmetry

TABLE 1. Chemical data for parisite-(La).

University of Arizona						
Constituent	wt.%	Range	Stand. dev.	Probe standard**	Crystal	Line
CaO	10.10	10.05–10.15	0.02	wollastonite	PET	Kα
Y <sub>2</sub> O <sub>3</sub>	0.52	0.47–0.55	0.02	YAG	TAP	Lα
La <sub>2</sub> O <sub>3</sub>	24.77	24.54–24.96	0.11	REE3	LIF	Lα
Ce <sub>2</sub> O <sub>3</sub>	11.16	11.03–11.32	0.07	REE3	LIF	Lα
Pr <sub>2</sub> O <sub>3</sub>	4.73	4.63–4.91	0.06	REE3	LIF	Lβ
Nd <sub>2</sub> O <sub>3</sub>	15.82		0.09	REE2	LIF	Lβ
Sm <sub>2</sub> O <sub>3</sub>	1.25		0.03	REE2	LIF	Lβ
Eu <sub>2</sub> O <sub>3</sub>	0.07		0.03	REE1	LIF	Lβ
F	7.30		0.18	MgF <sub>2</sub>	TAP	Kα
CO <sub>2</sub> calc	24.50					
–O = F	–3.07	–	–			
Total	97.15					
Universidade Federal de Minas Gerais						
CaO	9.45	9.28–9.73	0.16	wollastonite	PETJ	Kα
Y <sub>2</sub> O <sub>3</sub>	0.51	0.48–0.54	0.02	YAG	TAP	Lα
La <sub>2</sub> O <sub>3</sub>	24.82	24.31–25.32	0.41	monazite-(Ce)	PETJ	Lα
Ce <sub>2</sub> O <sub>3</sub>	12.99	12.86–13.24	0.16	monazite-(Ce)	PETJ	Lα
Pr <sub>2</sub> O <sub>3</sub>	7.95	7.27–8.83	0.53	monazite-(Ce)	LIF	Lβ
Nd <sub>2</sub> O <sub>3</sub>	14.77	14.23–15.26	0.38	monazite-(Ce)	LIF	Lβ
Sm <sub>2</sub> O <sub>3</sub>	1.24	1.22–1.27	0.02	monazite-(Ce)	LIF	Lβ
Eu <sub>2</sub> O <sub>3</sub>	0.07	0.02–0.09	0.03	monazite-(Ce)	LIF	Lβ
F	6.71	6.01–7.58	0.48	MgF <sub>2</sub>	TAP	Kα
CO <sub>2</sub> calc	24.70	–	–			
–O = F	–2.82	–	–			
Total	100.39					

\*\*Probe standard compositions (in wt.%): YAG = Y: 44.93, Al: 22.73, O: 32.34

REE1 = Si: 12.60, Al: 16.15, Ca: 17.98, Eu: 3.8, Gd: 3.87, Tb: 3.78, Tm: 3.81, O: 38.01

REE2 = Si: 12.65, Al: 16.21, Ca: 18.05, Nd: 3.65, Sm: 3.67, Yb: 3.74, Lu: 3.75, O: 38.27

REE3 = Si: 12.69, Al: 16.26, Ca: 18.1, Y: 3.21, La: 3.65, Ce: 3.42, Pr: 3.79, O: 38.88

(pseudo-trigonal) and systematic absences compatible with space groups  $C2$  (#5),  $Cm$  (#8),  $C2/m$  (#12). Single-crystal X-ray diffraction studies carried out using a Bruker APEX2 CCD automated diffractometer with graphite-monochromatized  $MoK\alpha$  ( $\lambda = 0.71073 \text{ \AA}$ ) radiation gave the following results:  $a = 12.356(1) \text{ \AA}$ ,  $b = 7.1368(7) \text{ \AA}$ ,  $c = 28.299(3) \text{ \AA}$ ,  $\beta = 98.342(4)^\circ$ ,  $V = 2469.1(4) \text{ \AA}^3$  and  $Z = 12$ . The  $a : b : c$  ratio calculated from the unit cell parameters is 1.7313 : 1 : 3.9652. Gladstone-Dale is  $-0.046$  (good) for the chemical analysis made in Arizona and  $-0.032$  (excellent) (Mandarino, 1981) for the chemical analysis made in Minas Gerais.

We confirmed that the space groups  $C2/c$  (#15) and  $Cc$  (#9) cited by Ni *et al.* (2000) were not consistent for parisite-(La). The space group  $C2/c$  (#15) analysis shows 816 reflections satisfying systematic absence conditions with an average  $I/s(I)$  of 2.07 (21,518 reflections read) and for the space group  $Cc$  (#9), there are 789 reflections with an average  $I/s(I)$  of 2.11 at the same conditions (20,612 reflections read).

For TEM studies, the sample was ground in an agate mortar and dispersed in a small volume (1 mL) of isopropanol. The suspension was dropped onto the carbon-coated Cu-TEM grid (300 mesh), and placed in a desiccator before TEM analysis. CBED and Nano-Beam Electron Diffraction (NBED) were performed by using a Tecnai G2-20 TEM (FEI), with a  $LaB_6$  filament,

operated at 200 kV, at the Center of Microscopy at UFMG, Belo Horizonte, Brazil. The diffraction patterns were recorded by using a side-mounted ES500W Erlangshen CCD camera (Gatan). The CBED patterns were performed using a convergence semi-angle of 1.3 mrad, with a beam size of  $\sim 20 \text{ nm}$ , and the NBED conditions were achieved by slightly spreading the  $C2$  condenser lens to obtain a nearly parallel narrow beam.

In order to deduce the crystal system, the Bravais lattice, and the possible space group, electron diffraction experiments were carried out following Morniroli and Steeds (1992), Redjaïmia and Morniroli (1994), Jacob *et al.* (2012) and Morniroli (2013). A suitable area of the sample was illuminated by a focused narrow beam under the TEM. Observations of CBED patterns were done while the sample was being tilted around a chosen Kikuchi line, or a row containing reflections, which passed through the origin of the reciprocal lattice. Several zone axis patterns (ZAPs) were recorded in the CCD until the ZAP of highest 'net'-symmetry had been found. The 'net'-symmetry takes into account the position of the reflections observed in the diffraction pattern, not their intensity. It is defined as the symmetry of the spots 'net' displayed in the zeroth order Laue zone (ZOLZ) and the whole pattern (WP), which includes the ZOLZ and first order Laue zone (FOLZ) (Morniroli and Steeds, 1992; Jacob *et al.*, 2012). Following Morniroli and Steeds (1992), the 'net'-symmetry

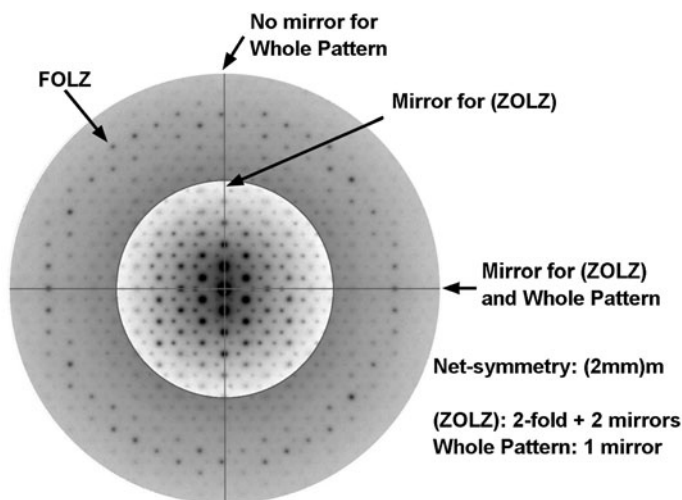


FIG. 6. Electron diffraction zone axis pattern of highest 'net' symmetry found in parisite-(La), required for the identification of the crystal system.

is here referred as '(ZOLZ)WP' symmetry – the (ZOLZ) symmetry is put in brackets henceforth in order to distinguish it from the WP's.

The identification of the monoclinic crystal system was achieved by observing the ZAP of highest 'net'-symmetry shown in Fig. 6. The two perpendicular axes drawn in the pattern (Fig. 6) indicate 2 mirrors, and also 2-fold axes, for the spots net shown in the ZOLZ, therefore the symmetry is  $(2mm)$ . The vertical axis shown in Fig. 6, however, is not a mirror for the WP, but the horizontal one. So the 'net'-symmetry observed in

this ZAP is  $(2mm)m$ . Comparisons with the Atlas of Electron Diffraction Zone-Axis Pattern (Momioli, 2013) showed that the ZAP shown in Fig. 6 corresponds to the  $[u0w]$  zone axis for the monoclinic system.

The non-primitive  $mS$  ( $mA$  or  $mB$ ) Bravais lattice was deduced by comparing the features displayed in the diffraction pattern shown in Fig. 7 with the typical ZAPs for the monoclinic crystal system (Momioli, 2013). The Fig. 7a shows the ZOLZ reflections of the either  $[010]_b$  or  $[001]_c$  zone axis, on which two symmetry axes are drawn – the

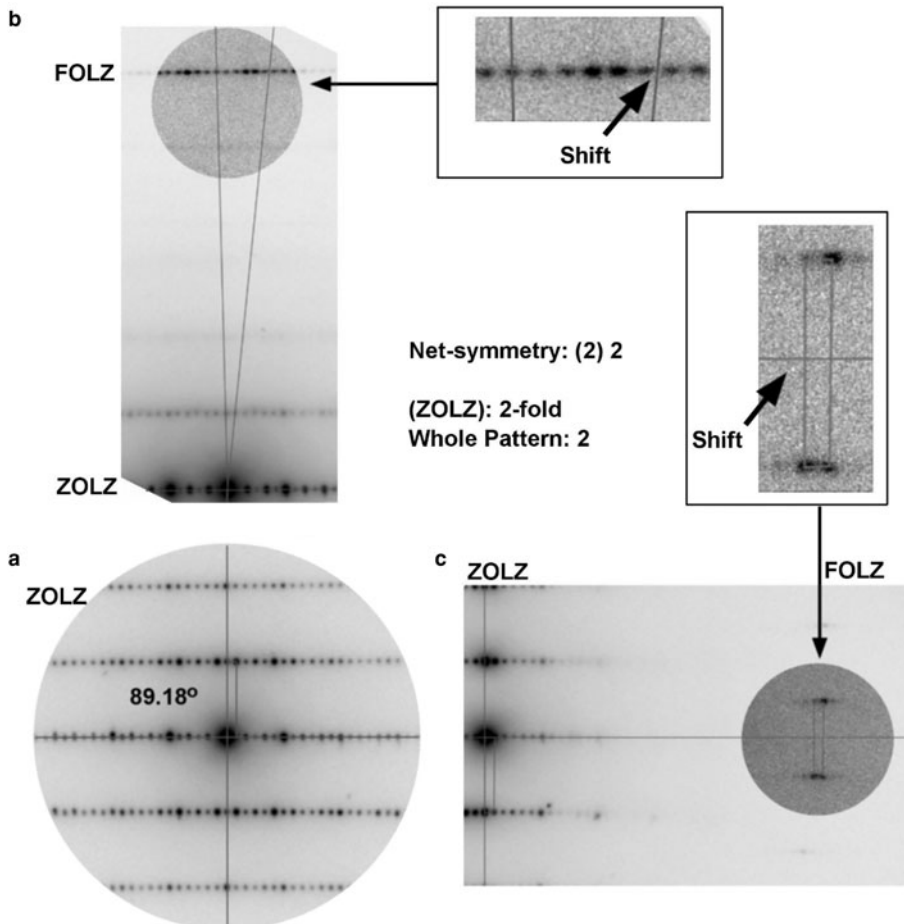


FIG. 7. Electron diffraction of the either  $[010]_b$  or  $[001]_c$  zone axis required for the identification of the Bravais lattice for the monoclinic crystal system. (a) Only the ZOLZ reflections are visible. The lines indicate the symmetry axis in the pattern. (b–c) Both ZOLZ and FOLZ reflections are visible after the electron beam had been tilted along each axis shown in (a). The narrow parallelogram drawn in each figure corresponds to the 'unit' cell in reciprocal space in the ZOLZ and FOLZ. The relative shift of the 'unit' cell in the FOLZ, along each symmetry axis, compared to the ZOLZ is an evidence for a non-primitive crystal system. There is no periodicity difference between ZOLZ and FOLZ reflections.



subscripts *b* and *c* stand for unique axis *b* and *c*, respectively. These non-perpendicular axes (beta\* or gamma\* equal 89.18°) indicate the 2-fold symmetry (2) for the spots net seen in the ZOLZ. The FOLZ reflections were not easily observed at first, so the electron beam was tilted along each axis until the FOLZ reflection could be seen at the microscope screen as shown in Figs 7*b* and *c*. From the observation of the FOLZ reflections the symmetry of the WP was taken as 2-fold. So the 'net'-symmetry of this ZAP concluded as (2)2. This is the exact zone axis pattern required for the identification of the Bravais lattice for the monoclinic system (Morniroli, 2013).

The narrow parallelograms drawn in the ZOLZ and FOLZ reflections shown in Fig. 7 correspond to the 'unit' cell in the reciprocal space. This 'unit' cell indicates the periodicity of reflections in the spots net in the diffraction pattern. As can be seen in Fig. 6, there is a relative shift of the 'unit' cell in the FOLZ compared to the ZOLZ. This means that the Bravais lattice of the parasite-(La) crystal is non-primitive (Morniroli and Steeds, 1992; Jacob *et al.*, 2012). Therefore, the Bravais lattice is *mS* (*mA* or *mB*).

The lack of periodicity differences between ZOLZ and FOLZ reflections is evidence that there are no glide planes parallel to [010]<sub>*b*</sub> or

TABLE 2. Powder X-ray diffraction data of parasite-(La).

<i>I</i> <sub>obs</sub>	<i>d</i> <sub>obs</sub> , Å	<i>d</i> <sub>calc</sub> , Å	<i>hkl</i> *
55	13.95	13.991	002
20	6.98	6.995	004
37	4.655	4.664	006
88	3.555	3.561, 3.558	020, $\bar{3}11$
13	3.446	3.451, 3.449, 3.448	022, 311, $\bar{3}13$
3	3.323	3.326, 3.325, 3.324	023, 312, $\bar{3}14$
18	3.169	3.173, 3.172, 3.171	024, 313, $\bar{3}15$
12	3.000	3.004, 3.003, 3.002	025, 314, $\bar{3}16$
100	2.827	2.830, 2.829, 2.828	026, 315, $\bar{3}17$
2	2.655	2.659, 2.658, 2.657, 2.657	027, 316, $\bar{3}18$ , 404
2	2.495	2.495, 2.495, 2.494	028, 317, $\bar{3}19$
8	2.331	2.332	0.0.12
1	2.274	2.275, 2.274, 2.271	$\bar{1}33$ , 424, $\bar{2}29$
2	2.241	2.246, 2.245	133, 422
10	2.199	2.200, 2.200, 2.199	0.2.10, 319, $\bar{3}.1.11$
58	2.055	2.055, 2.054	$\bar{3}31$ , $\bar{6}02$
4	2.034	2.033, 2.032, 2.032	$\bar{3}33$ , 600, 604
6	1.971	1.972, 1.972, 1.971, 1.971	$\bar{3}33$ , $\bar{3}35$ , 602, $\bar{6}06$
38	1.950	1.951, 1.951, 1.950	0.2.12, 3.1.11, $\bar{3}.1.13$
36	1.880	1.881, 1.881, 1.880, 1.879	$\bar{3}35$ , $\bar{3}37$ , 604, $\bar{6}08$
9	1.780	1.780, 1.779	040, $\bar{6}22$
2	1.767	1.772, 1.772, 1.771	337, $\bar{3}39$ , 6.0.10
1	1.749	1.749	0.0.16
3	1.725	1.725, 1.724, 1.724	044, 622, $\bar{6}26$
23	1.663	1.663, 1.662, 1.662	046, 624, $\bar{6}28$
3	1.570	1.570, 1.570, 1.569	0.2.16, 3.1.15, $\bar{3}.1.17$
12	1.542	1.542, 1.542, 1.542, 1.541	3.3.11, 3.3.13, 6.0.10, $\bar{6}.0.14$
2	1.502	1.502, 1.502, 1.501	0.4.10, 628, $\bar{6}.2.12$
9	1.425	1.425, 1.425, 1.424	0.2.18, 3.1.17, $\bar{3}.1.19$
9	1.415	1.415, 1.415, 1.414	0.4.12, 6.2.10, $\bar{6}.2.14$
9	1.346	1.346, 1.345, 1.345	$\bar{3}51$ , 642, $\bar{9}13$
3	1.332	1.332, 1.332, 1.332	3.3.15, 6.0.14, $\bar{3}.3.17$

\*The *hkl* indices are chosen taking into account intensities of reflections of the powder X-ray diffraction pattern calculated from the structure data for monoclinic parasite-(Ce) reported by Ni *et al.* (2000).

TABLE 3. Comparative data for parisite-(La) and parisite-(Ce).

	Parisite-(La) CaLa <sub>2</sub> (CO <sub>3</sub> ) <sub>3</sub> F <sub>2</sub>	Parisite-(Ce) CaCe <sub>2</sub> (CO <sub>3</sub> ) <sub>3</sub> F <sub>2</sub>
Formula		
Space group	<i>C2, Cm, C2/m</i>	<i>C2/c</i> or <i>Cc</i>
Unit-cell parameters	<i>a</i> = 12.3563(13) <i>b</i> = 7.1368(7) <i>c</i> = 28.299(3) Å $\beta$ = 98.342(4)° <i>Z</i> = 12	<i>a</i> = 12.305(2) <i>b</i> = 7.1053(5) <i>c</i> = 28.250(5) $\beta$ = 98.257(14)° <i>Z</i> = 12
Strongest lines of the powder X-ray diffraction pattern: <i>d</i> , Å ( <i>I</i> , %)	2.827(100), 3.555(88), 2.055(58), 13.95(55), 1.950(38), 4.655(37), 1.880(36)	3.565(100), 2.838(100), 2.060(80), 1.938(60), 1.882(50), 1.658(50), 14.03(40)
Optical data:	$\omega$ = 1.670(2)	$\omega$ = 1.6718–1.6767
Optical sign	$\epsilon$ = 1.782(5) (+)	$\epsilon$ = 1.7664–1.7729 (+)
Density, g cm <sup>-3</sup>	4.331	4.3915
Mohs hardness	4–5	4½
References	This study	Cell data: Ni <i>et al.</i> (2000); PXRD: Cheang (1977); optical data, density, hardness: Flink (1901)

[001]<sub>c</sub> (Mornioli and Steeds, 1992; Jacob *et al.*, 2012) as reported by Ni *et al.* (2000) for parisite-(Ce). It was not possible to deduce the screw axis perpendicular to the zone axis pattern [u0w] shown in Fig. 6. The possible 2<sub>1</sub> screw axis perpendicular to that particular zone axis could be related to the forbidden reflections in the row defined by any of the symmetry axes shown in Fig. 6. The forbidden nodes would appear, however, to be due to a double diffraction effect. This could be investigated by tilting the beam around the symmetry axis shown in Fig. 6 in order to decrease the intensity of the probable forbidden reflections (Mornioli and Steeds, 1992), but it has been not verified during measurements. Moreover, the absence of glide planes parallel to [010]<sub>b</sub> or [001]<sub>c</sub> are consistent with the possible extinction symbols, *A1-1<sub>b</sub>* or *B11-<sub>c</sub>*. From the comparisons of the features observed in the experimental ZAPs with the typical theoretical diffraction patterns (Mornioli, 2013), the possible space groups are *A121* (#5), *A1m1* (#8), *A12/m1* (#12), *B112* (#5), *B11m* (#8) or *B112/m* (#12), alternative settings of the space groups *C2* (#5), *Cm* (#8), *C2/m* (#12).

Unfortunately, despite determining monoclinic unit-cell parameters from the single-crystal pattern, we could not obtain single-crystal data suitable for the structure refinement. Thin inclusions are visible under the microscope. It is possible they are the main cause of the absence of single crystals suitable

for structural investigations. Inclusions of synchysite, röntgenite or bastnäsite microblocks are typical for parisite in general.

Powder X-ray diffraction data (Table 2) were obtained using a Rigaku R-Axis Rapid II single-crystal diffractometer equipped with cylindrical image plate detector using Debye-Scherrer geometry (*d* = 127.4 mm; CoK $\alpha$  radiation). Parameters of the monoclinic unit cell refined from powder data are: *a* = 12.323(7), *b* = 7.121(2), *c* = 28.28(1) Å,  $\beta$  = 98.33(4)° and *V* = 2456(3) Å<sup>3</sup>. A comparison of data for parisite-(La) and parisite-(Ce) is given in Table 3.

## Discussion

The second most abundant REE in parisite-(La) from Mula mine is Nd, not Ce. On a chondrite-normalized plot there would be a marked negative Ce anomaly. One hypothesis about the conditions of formation could be that the fluids that transported REE had leached them in a mildly oxidizing environment, where Ce was partially oxidized to Ce<sup>4+</sup> and thus remained immobile. The resulting solution would be depleted in Ce. For the other five parisite-(La) occurrences quoted in the literature, neither crystallographic nor chemical data are presented. The only exception is a partial chemical analysis for parisite-(La) from Třebíč durbachite

massif, SW Moravia, Czech Republic (Sulovský, 2001): La<sub>2</sub>O<sub>3</sub> 28.68, Ce<sub>2</sub>O<sub>3</sub> 24.07, Nd<sub>2</sub>O<sub>3</sub> 4.01, CaO 10.22, SO<sub>3</sub> 0.98, F 6.38, O = F -2.67, total 71.64 wt.%. The calculated formula is Ca<sub>1.01</sub>(La<sub>0.97</sub>Ce<sub>0.81</sub>Nd<sub>0.13</sub>)<sub>Σ1.91</sub>(CO<sub>3</sub>)<sub>2.89</sub>(SO<sub>4</sub>)<sub>0.07</sub>F<sub>1.84</sub>. In this case Ce is the second most abundant REE and the conditions of formation differ from that of parisite-(La) from Mula mine.

## Acknowledgements

We acknowledge the Brazilian agencies FAPESP (processes 2014/50819-9 and 2013/03487-8), CNPq, and Finep for financial support, all members of the IMA Commission on New Minerals, Nomenclature and Classification, the Principal Editor Peter Williams, an anonymous reviewer and Fernando Colombo and Peter Leverett for their helpful suggestions and comments. M. Chaves thanks CNPq (grant No. 305492/2013-6) and R. Scholz thanks CNPq and FAPEMIG (respectively grant No. 305284/2015-0 and grant APQ-01448-15).

## References

- Adler, H.H. and Kerr, P.F. (1963) Infrared spectra, symmetry and structure relations of some carbonate minerals. *American Mineralogist*, **48**, 839–853.
- Betancourt, V.M.R. (2003) *Raman Spectroscopic Study of High Temperature Rare Earth Metal – Rare Earth Halide Solutions: Ln–LnX<sub>3</sub>– and LnX<sub>2</sub>–LnX<sub>3</sub>–(LiX–KX)eu Systems (Ln: Nd, Ce; X: Cl, I)*. Dr. Sci. thesis. Faculty of Chemistry and Biosciences, Karlsruhe University, Germany.
- Cheang, K. (1977) *Structure and Polytypism in Synchysite and Parisite from Mont St. Hilaire, Quebec*. M.S. thesis, Carleton University, Ottawa, Canada.
- Enrich, G.E.R., Gomes, C.B. and Ruberti, E. (2010) Química mineral de carbonatos de elementos terras raras em nefelina sienitos e fonólitos apaiticos do maciço de Cerro Boggiani, Província Alto Paraguai, Paraguai. *X Congresso de Geoquímica dos Países de Língua Portuguesa, 2010, Porto. Actas, 2010*. v. CD-rom, pp. 223–227.
- Flink, G. (1901) Part I. On the minerals from Narsarsuk on the Firth of Tunugdliarfik in Southern Greenland. Parisite. *Meddelelser om Grønland*, **24**, 29–42.
- Frost, R.L. and Dickfos, M.J. (2007) Raman spectroscopy of halogen-containing carbonates. *Journal of Raman Spectroscopy*, **38**, 1516–1522.
- Frost, R.L., López, A., Scholz, R., Xi, Y. and Belotti, F.M. (2013) Infrared and Raman spectroscopic characterization of the carbonate mineral huanghoite – And in comparison with selected rare earth carbonates. *Journal of Molecular Structure*, **1051**, 221–225.
- Guastoni, A., Kondo, D. and Nestola, F. (2010) Bastnäsité-(Ce) and parisite-(Ce) from Mt. Malosa, Malawi. *Gems & Gemology*, **46**, 42–46.
- Hirtopanu, P. (2006) One hundred minerals for one hundred years (dedicated to the Centennial of the Geological Institute of Romania), 3rd Conference on Mineral Sciences in the Carpathians, Miskolc Hungary. *Acta Mineralogica–Petrographica, Abstract series*, **5**, 86.
- Hirtopanu, P., Fairhurst, R.J. and Jakab, G. (2015) Niobian rutile and its associations at Jolotca, Ditrau Alkaline Intrusive Massif, East Carpathians, Romania. *Proceedings of the Romanian Academy, Series B*, **17**, 39–55.
- Jacob, D., Ji, G. and Morniroli, J.P. (2012) A systematic method to identify the space group from PED and CBED patterns part II – practical examples. *Ultramicroscopy*, **121**, 61–71.
- Jambor, J.L., Burke, E.A., Ercit, T.S. and Grice, J.D. (1988) New mineral names. *American Mineralogist*, **73**, 1496–1497.
- Mandarino, J.A. (1981) The Gladstone–Dale relationship: Part IV. The compatibility concept and its application. *Canadian Mineralogist*, **19**, 441–450.
- Martins, A.A.M., Andrade Filho, E.L.A., Loureiro, H.S.C., Arcanjo, J.B.A. and Guimarães, R.V.B. (2008) *Geologia da Chapada Diamantina Oriental (Projeto Ibityara – Rio de Contas)*. Série Arquivos Abertos **31** – CPRM (Serviço Geológico do Brasil) and CBPM (Companhia Baiana de Pesquisa Mineral), Salvador, 64 pp.
- Menezes Filho, L.A.D., Chukanov, N.V., Rastsvetaeva, R. K., Aksenov, S.M., Pekov, I.V., Chaves, M.L.S.C., Richards, R.P., Atencio, D., Brandão, P.R.G., Scholz, R., Krambrock, K., Moreira, R.L., Guimarães, F.S., Romano, A.W., Persiano, A.C., Oliveira, L.C.A. and Ardisson, J.D. (2015) Almeidaite, Pb(Mn,Y)Zn<sub>2</sub>(Ti,Fe<sup>3+</sup>)<sub>18</sub>O<sub>36</sub>(O,OH)<sub>2</sub>, a new crichtonite-group mineral, from Novo Horizonte, Bahia, Brazil. *Mineralogical Magazine*, **79**, 269–283.
- Moore, M., Chakhmouradian, A.R., Mariano, A.N. and Sidhu, R. (2015) Evolution of rare-earth mineralization in the Bear Lodge carbonatite, Wyoming: Mineralogical and isotopic evidence. *Ore Geology Reviews*, **64**, 499–521.
- Morniroli, J.P. (2013) *Atlas of Electron Diffraction Zone Axis Patterns*, p. 314. Available at: <http://www.electron-diffraction.fr>.
- Morniroli, J.P. and Steeds, J.W. (1992) Microdiffraction as a tool for crystal structure identification and determination. *Ultramicroscopy*, **45**, 219–239.
- Nakamoto, K. (1997) *Infrared and Raman Spectra of Inorganic and Coordination Compounds. Part A: Theory and Applications in Inorganic Chemistry*. John Wiley and Sons, New York.
- Nakamoto, K. (2009) *Infrared and Raman Spectra of Inorganic and Coordination Compounds. Part A:*

- Theory and Applications in Inorganic Chemistry*. (Sixth edition). John Wiley and Sons, New Jersey.
- Ni, Y, Post, J.E. and Hughes, J.M. (2000) The crystal structure of parisite-(Ce),  $\text{Ce}_2\text{CaF}_2(\text{CO}_3)_3$ . *American Mineralogist*, **85**, 251–258.
- Pedrosa-Soares, A.C., Campos, C., Noce, C.M., Silva, L.C., Novo, T., Roncato, J., Medeiros, S., Castañeda, C., Queiroga, G., Dantas, E., Dussin, I. and Alkmim, F. (2011) Late Neoproterozoic–Cambrian granitic magmatism in the Araçuaí orogen (Brazil), the Eastern Brazilian Pegmatite Province and related deposits. Pp. 25–51 in: *Granite-Related Ore Deposits* (A.N. Sial, J.S. Bettencourt, C.P. De Campos, V.P. Ferreira, editors). Geological Society of London Special Publications, **350**.
- Ranieri, I.M., Baldochi, S.L. and Klimm, D. (2008) The phase diagram  $\text{GdF}_3$ – $\text{LuF}_3$ . *Journal of Solid State Chemistry*, **181**(5), 1070–1074.
- Redjaimia, A. and Morniroli, J.P. (1994) Application of microdiffraction to crystal structure identification. *Ultramicroscopy*, **53**, 305–317.
- Sulovský, P. (2001) Accessory minerals of the Třebíč durbachite massif (SW Moravia). *Mineralia Slovaca, Košice: SGS*, **33**(5), 467–472.
- Teixeira, L.R. (2005) *Projeto Ibitiara – Rio de Contas, Estado da Bahia. Programa Recursos Minerais do Brasil, Litogeoquímica*. CPRM (Serviço Geológico do Brasil) and CBPM (Companhia Baiana de Pesquisa Mineral), Salvador, 33 pp. + xv.
- Theye, T., Ockenga, E. and Bertoldi, C. (2003) Davidite (-La), bastnaesite(-La), parisite(-La), monazite(-La): REE minerals at a metabauxite/marble interface in eastern Samos (Greece). *Berichte der Deutschen Mineralogischen Gesellschaft, Beihefte zum European Journal of Mineralogy*, Vol. **15** (1). <ftp://ftp.gmg.rub.de/pub/geo2003/17%20Quantification%20and%20dating%20of%20metamorphic%20processes%20WILLNER/Theye.PDF>.
- White, W.B. (1974) The carbonate minerals. Pp. 227–284 in: *Infrared Spectra of Minerals* (V.C. Farmer, editor). Mineralogical Society Monograph, **4**. London.